Microchimica Acta (2018) 185: 171
https://doi.org/10.1007/s00604-018-2676-y

ORIGINAL PAPER

Gold nanoclusters as a quenchable fluorescent probe for sensing oxygen at high temperatures

Alba Martín-Barreiro[1] · Susana de Marcos[1] · Javier Galbán[1]

Received: 18 October 2017 / Accepted: 11 January 2018 / Published online: 13 February 2018

Abstract

Gold nanoclusters (AuNCs) capped with lipoic acid (LA) or templated with bovine serum albumin (BSA) are shown to be viable fluorescent probes for oxygen (O_2) which acts as a collisional quencher. Quenching of fluorescence, with its lifetimes in the order of 123 ± 9 ns (LA) and 153 ± 15 ns (BSA) (in aqueous solution), is best measured at excitation/emission wavelengths of 400/680 nm and 375/650 nm respectively. It follows the Stern-Volmer model, whose quenching constants (K_{sv}) and quenching efficiencies (γ) are 1400 M^{-1} and 0.52 for AuNC@LA and 4479 M^{-1} and 0.90 for AuNC@BSA. The probes were immobilized on a silica support and tested for response to O_2 in gas phase using a commercial instrument. The effect of temperature on the fluorescence of AuNC@LA was studied in the range from 30 to 210 °C. Fluorescence intensity slightly decreases with temperature in the first heating cycle but remains constant in further cycles. The AuNC@LA were studied for their response to O_2 in the temperature range from 30 to 100 °C, and even at 100 °C they respond to O_2, with a K_{sv} that slightly drops with increasing temperature. Measuring in gas phase at 100 °C, the sensor has a detection limit of 3% (V/V) of O_2 at a signal-to-noise ratio of 3.

Keywords Fluorescence quenching · Collisional quenching · Oxygen sensor · BSA-template · Lipoic acid-capped · Commercial device · Elevated temperature · Stern-Volmer equation · Nanomaterial

Introduction

Gold nanoclusters (AuNCs) are perhaps the kind of NCs which are acquiring more importance in analytical chemistry because of their interesting optical properties [1, 2]. Like other nanomaterials (such as quantum dots), their Stokes' shift and emission peaks (λ_{em}) depend on the number of gold atoms forming the AuNCs. However, for larger AuNCs, the λ_{em} also depends on the ligand used for AuNC stabilization, i.e., the chemical pathway used for their synthesis so that variations in the synthesis method usually produce modifications in their spectroscopic properties.

The analytical applications of AuNCs fluorescence for sensing and bioimaging [3] have become more widespread [4–6]. According to Li et al. [6], these methods are mainly based on three mechanisms: 1) fluorescence quenching, which is the basis of the determination of ion metals such as Hg(II) and Cu(II), or small molecules such as dopamine [7] or histamine; 2) AuNCs aggregation for protein determination; and 3) energy transfer (FRET) for bioimaging. Unlike other nanomaterials [8, 9], AuNCs have been scarcely used to sense gases.

O_2 determination is one of the most interesting real world applications of molecular luminescence [10–14]. Compared to other sensing principles, as the amperometric Clark electrode or the Lambda sensor, present several advantages as the possibility of remote and non-invasive sensing, greater miniaturization, analyte imaging and the lack of analyte consumption [10]. Although a mechanism assisted by O_2 singlet and luminophore triplet assisted (O_2*-T) has been described demonstrating that O_2 can produce fluorescence enhancement in some compounds [15, 16], these methods are generally based on the collisional quenching that the analyte produces in the excited state, so reagents having long luminescent (fluorescence or phosphorescence) lifetimes are used. For this application, probes have been proposed [10, 11] such as polycyclic aromatic hydrocarbons, fullerenes and especially different kinds of metal-ligands complex, being those based on Ru-dilphenylphenanthroline and Pt or Pd tetrakisfluorophenyl porphyrins (PtTFPP or PdTFPP) which present better analytical figures of merit and applicability,

Electronic supplementary material The online version of this article (https://doi.org/10.1007/s00604-018-2676-y) contains supplementary material, which is available to authorized users.

✉ Javier Galbán
jgalban@unizar.es

[1] Analytical Biosensors Group, Analytical Chemistry Department, Faculty of Sciences, Instituto Universitario de Nanociencia de Aragon (INA), University of Zaragoza, Pedro Cerbuna 12, 50009 Zaragoza, Spain

and being the reagent of choice in different commercial O_2 monitoring systems.

Some types of nanomaterials, especially nanoclusters having long luminescence lifetimes, are also potential candidates for O_2 sensing. However, very few references can be found in the literature addressing this possibility (the paper by Ghost et al., using Mo chloride NCs being an exception [17]) and none of these few papers mention collisional quenching to explain the O_2 effect in AuNCs. Thus, Wang [18] designed a fluorescence biosensor for proteases based on the degradative effect of these proteins on AuNC@BSA; after the degradation, O_2 comes into the reagent and the Au fluorescence becomes quenched by a mechanism not clearly explained. Das et al. [19], studied the O_2 effect on two AuNC@BSA (2 nm and 2.5 nm in diameter) having blue (410 nm) and red (645 nm) fluorescence respectively; the authors found a fluorescence enhancement in the blue AuNCs, explained by the O_2*-T mechanism, and fluorescence quenching in the red ones, due to AuNCs aggregation.

O_2 sensing at high temperatures is important in several applications as automotive industry, power generation, food processing or chemical and biochemical reactors. For these proposals, O_2 sensors based on organic fluorophores present limited applications. In this paper, we study the fluorescence quenching caused by O_2 in two different types of AuNCs, in the light of the Stern-Volmer model at ambient temperature. Because of their metallic nature, AuNCs also tolerate elevated temperatures, leading to their use as O_2 sensors at higher temperature that organic fluorophores, an aspect also evaluated in this paper.

Experimental

Reagents

Hydrogen tetrachloroaurate (III) hydrate (99.8%-Au) ($AuCl_4Na.2H_2O$) was purchased from Stream Chemicals (https://secure.strem.com). Sodium borohydride and (±)-α-lipoic acid, were purchased from Sigma-Aldrich Co. LLC. (http://www.sigma-aldrich.com). Alphagaz1 (99.999%) compressed oxygen and nitrogen, were purchased from Air Liquide (Madrid, Spain, https://industrial.airliquide.es/). Precoated TLC-sheets Polygram Sil G and DC-Fertigfolien Alugram Sil G were purchased from Macherey-Nagel (Düren, Germany, https://www.mn-net.com/).

Apparatus

Purification of the synthetized gold nanoclusters (AuNCs) was carried out using a Koch centrifuge from Bunsen (Spain, http://www.bunsen.es) and Amicon-Ultra 10 kDa centrifugal filters from Millipore (Germany).

A Tecnai F30H–7650 microscope (scanning and transmission mode, STEM) (FEI, The Netherlands, https://www.fei.com) was used for AuNCs characterization.

Steady state fluorescence measurements were carried out with a Photon Technology International (PTI) Time Master fluorescence spectrometer (TM-272003). For lifetime measurements this instrument has a N_2 laser (GL-3300) that pumps a dye laser, as a radiation source, and a stroboscopic system as the detector.

A Foxy-R fluorescence O_2 sensor from Ocean Optics (EW Duiven, The Netherlands, https://oceanoptics.com/) consisted of a QE65000 CCD-array spectrometer coupled to an oxygen probe FOXY-R (by a QBIF600-UV/Vis optical fiber), using a blue LED light pulsed Ocean Optics LS-450 as radiation source. This sensor was calibrated in gas phase (and in solution (ESM 1, Fig. S1.1 and S1.2) with the help of the visocolor ECO Test 5–88 for O_2 (Macherey-Nagel) which is based in the classical Winkler method.

LS-450 light source and QE65000 CCD-array spectrometer coupled to a QF600–8-VIS/NIR optical fiber was used for AuNC fluorescence measurements.

A LuminOx™ gas phase optical oxygen sensor (static type) from SST (www.sstsensing.com) consisting of a 420 nm excitation LED, a photodiode (Fig. 2) and a Ruthenium compound as the sensing element. This sensor measures O_2 concentration from 0 to 25% (V/V) (see ESM1, Fig. S1.3 for original sensor calibration).

For high temperature AuNC fluorescence measurements, the optical fiber illuminated (across a quartz transparent window) a homemade heating system (Pervaporator) previously described [20] (ESM2, Fig. S2.1). In brief, the system consists of a measuring chamber with two quartz windows. The system is heated using a cylindrical resistance and the temperature is controlled by a home-made digital controller (accuracy, ±1 °C). The maximum temperature provided by the resistance was 250 °C. The whole pervaporator was placed on a PTFE support.

Gold nanoclusters synthesis

Lipoic acid stabilized gold nanoclusters (AuNC@LA) were synthesized by a chemical reduction method using $NaBH_4$ as the reducer and lipoic acid as the capping agent, applying a previously described procedure [21] (ESM 3.1). Albumin bovine gold nanoclusters (AuNC@BSA) were also synthesized according to the procedure described by Lianzhe et al. [22] (ESM 4.1).

Fluorescence characterization and O_2 effect on AuNCs in batch

The effect of the O_2 on AuNC fluorescence was monitored with the PTI in Timebased mode, using the

following instrumental conditions (excepting where indicated): 15 nm excitation and fluorescence slits, 1000 nm min^{-1} scanning speed, measured at λ_{exc} /λ_{flu}, 400/680 nm (for AuNC@LA) and 375/650 nm (for AuNC@BSA). Gas flows of different oxygen concentrations were pumped through the cuvette containing AuNCs and the fluorescence variation was continuously measured over time. The average fluorescence intensity value was taken. In parallel, the O_2 concentration was monitored using the Foxy-R fluorescence sensor.

Measurements of fluorescence decays were performed with a pulsed dye laser. The N_2 laser pumped the dye PLD457, which emits in the range from 440 to 478 nm with a maximum at 457 nm. The following instrumental parameters were applied: 100 ns offset, 1000 μs integration time, 20 averages (complete offset intervals) with 5 shots at each offset for each of the sweeps performed and 10 Hz frequency of firing of the laser. From the fluorescence decay and lamp profile registers, the lifetimes were calculated both manually and through the program by adjustment to a function.

Immobilization of AuNCs on silica support

AuNCs were immobilized either: 1) on pre-coated TLC-sheets Polygram SilL G, in which the silica is supported on polyethylene and whose transparency allows to implement them in an optical sensor, and 2) on pre-coated DC- Fertigfolien Alugram Sil G, a silica supported on aluminum and suitable for studies at temperature higher than 25 °C. In both cases, the immobilization was carried out by immersing the TLC-sheets in a preconcentrated solution of nanoclusters (840 mg mL^{-1} Au) and allowing the system to dry at room temperature; to obtain homogeneous deposition, three immersion/drying cycles were applied.

Fluorescence characterization and O_2 effect of AuNCs immobilized on silica support

The emission spectra at ambient temperature of the AuNCs immobilized on silica support, were carried out with the QE65000 spectrometer coupled to the QF600–8-VIS/NIR optical fiber.

To study the O_2 effect, the Ruthenium fluorophore initially placed in the the LuminOx™, was replaced by the AuNCs-silica platform (cut to an appropriated size). The whole system was then inserted into a homemade chamber consisting of a PVC vessel with inlet and outlet for gases (ESM2, Fig. S2.2). In parallel to these measurements, the O_2 in the chamber was monitored with the FOXY-R oxygen probe in order to know the concentrations of O_2 in each moment.

Measurement of the AuNCs-silica platform fluorescence at high temperature: O_2 effect

AuNC@LA immobilized onto the silica support were placed in the measuring chamber of the pervaporator. The variation of the fluorescence intensity with the temperature was monitored with the QE65000 spectrometer coupled to the optical fiber QF600–8-VIS/NIR.

Results and discussion

AuNCs characterization

The synthesized AuNC@LA were characterized by STEM; the images showed spherical morphology and homogeneous particles, with an average diameter of 1.60 ± 0.23 nm (ESM3.2, Fig. S3.1). The gold content in the AuNCs stock was obtained by ICP-AES resulting in 0.28 gL^{-1}. The excitation and fluorescence maximum of these AuNCs appear at 400 nm and 680 nm, respectively (Fig. 1A). The wavelength of the maximum excitation slightly depended on the AuNCs concentration but not the fluorescence spectra (ESM3.3, Fig. S3.2); the fluorescence lifetime of these nanoclusters was 123 ± 9 ns (in aqueous solution at $2.2 \cdot 10^{-4}$ M O_2) which enables the use of these nanomaterials as O_2 fluorescence probes to be evaluated.

Similar studies were performed with AuNC@BSA. The STEM image (ESM4.1, Fig. S4.1) also showed spherical morphology with a mean diameter of 1.80 ± 0,35 nm (and large masses of protein surrounding the nanoclusters). AuNC@BSA showed excitation and emission maxima at 375 nm and 650 nm, respectively (Fig. 1B) and its fluorescence lifetime was 153 ± 15 ns (in aqueous solution at $2.2 \cdot 10^{-4}$ M O_2).

Chevrier et al. [23] found that AuNCs have low photobleaching. Our results agree with these observations: AuNC@LA did not show photobleaching during at least 3 h under continuous excitation; in the same experimental conditions, AuNC@BSA showed a slight instability during the first 1.5 h but during the following 1.5 (at least) the fluorescence remained constant. (ESM3.4, Fig. S3.3).

The fluorescence quantum yield (Φ) for both types of AuNCs was obtained using tris(bipyridine)ruthenium(II) chloride as a reference standard. Values of 0.018 (see ESM3.5) and 0.089 (ESM 4.3) for AuNC@LA and AuNC@BSA were obtained which reasonably agree with those previously reported in the bibliography of 0.018 [24] and 0.080 [25], respectively. These yields are comparable to those of organic fluorophores and they are in the range of what is necessary for their application as optical sensors.

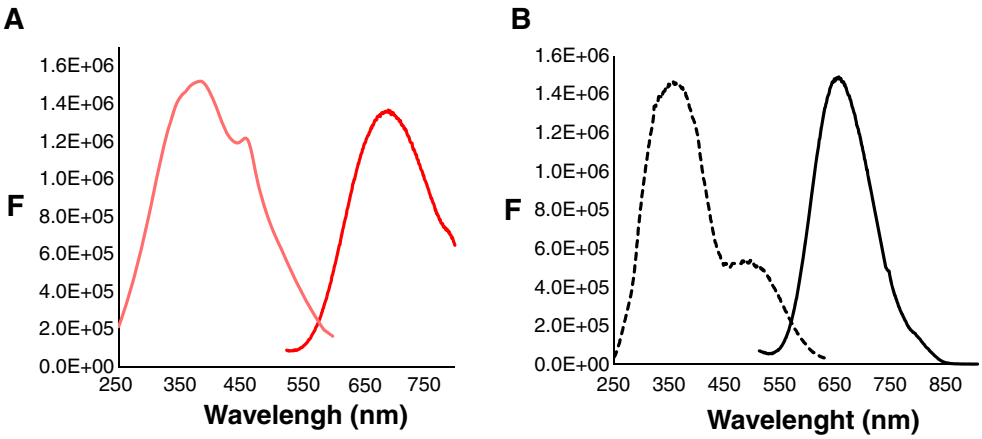

Fig. 1 Excitation (left) and emission (right) spectra of AuNCs in solution. **A**) AuNC@LA (λ_{ext} = 400 nm and λ_{em} = 680 nm) **B**) AuNC@BSA (λ_{ext} = 375 nm and λ_{em} = 650 nm). Other instrumental conditions as indicated in the Experimental section

AuNC fluorescence quenching in solution

The effect of the O_2 concentration on the AuNC@LA fluorescence was first studied in solution following the procedure explained in the Experimental section. The results led us to conclude that:

1) The O_2 fluorescence quenching fits the conventional Stern-Volmer eq. (1) and not the modified equation for two populations of fluorophores (accessible and not accessible). This result is consistent with the idea of nanoclusters behave as an entity with a specific energy level structure. The Stern-Volmer constant (K_{sv}) is independent of the AuNC@LA concentration used. Five K_{sv} values were obtained using different AuNC@LA concentrations (ESM3.6, Fig. S3.6, Table S3.1). The average value obtained was 1400 M^{-1} (RSD = 8.8%). This K_{sv} is smaller than that obtained for the Ru(II) complex of the Foxy-R probe which is consistent with its lower fluorescence lifetime.
2) The lifetime values obtained for three O_2 concentrations (ESM3.7, Table S3.2), confirm that the quenching follows a collisional mechanism (1). The K_{sv} obtained from lifetime measurements was 1346 M^{-1} (RSD = 10%) which statistically (t-test, 95% confidence) agrees with the value measured from the intensity values (1400 M^{-1}).

$$\frac{F_0}{F} = \frac{\tau_0}{\tau} = 1 + K_{sv}[O_2] = 1 + k_0\gamma\tau_0[O_2] \quad (1)$$

3) The O_2 quenching efficiency (γ) on the AuNC@LA fluorescence was estimated to be 0.52 (ESM5.1), which is lower than that of most of molecular fluorophores (≈1), and is also consistent with the idea that the energy levels responsible for the fluorescence are partially shielded by this AuNCs structure.
4) The quenching is fully reversible. Fig. S3.7 (ESM3.8) gives the fluorescence intensity variations obtained with consecutive N_2-O_2 flow cycles, although more complete additional results dealing with the reversibility of the sensor will be given in gas phase.

Similar studies were carried out with AuNC@BSA. A higher sensitivity to O_2 quenching was observed with these nanoclusters compared to AuNC@LA with a 4479 M^{-1} K_{sv} value (RSD = 10.0%, n = 3) (ESM4.2, Fig. S4.2) only half of that obtained with the Foxy sensor, and a quencher efficiency of 0.9 (ESM5.2). Considering that the O_2 accessibility to the energy levels of both types of nanocluster is the same, this higher efficiency can be explained considering that in BSA, the nanoclusters are close to each other (see Figs. S3.1 and S4.1), giving higher apparent kinetic radium and shortening the mean pathway for the oxygen between collisions. The K_{sv} value was also calculated from lifetime measurements, obtaining 3576 M^{-1} (RSD = 9.8%, n = 3) (ESM4.4). This value was statistically compared to that obtained by fluorescence intensity (t-test); a $t_{experimental}$ of 2.75 was obtained, which is nearly the limit at 95% confidence (t = 2.78) and higher than that at 90%; the differences between these K_{sv} values is attributed to the difficulty of reproducing laser operation conditions.

Immobilization of the AuNCs to obtain solid state sensors in gas phase: read-out possibilities

Once the viability of an effective O_2 quencher was tested, the possibility of using this effect for designing an O_2 gas sensor was studied. AuNC@LA were immobilized on a silica support following the previously described procedure. This platform showed worse-defined excitation and emission spectra than those obtained in solutions, due to both the nature of the support and the design of the system used for measuring (ESM6.1, Fig. S6.1).

AuNC@LA immobilized on the silica support was tested as the chemical basis of the Luminox™ O_2 sensor (Fig. 2) described in the experimental section. For the calibration of

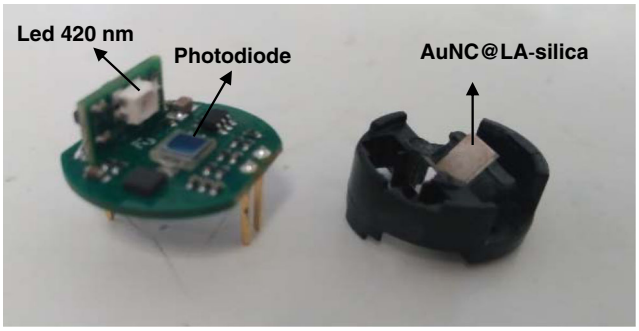

Fig. 2 Commercial optical sensor with AuNCs on a silica support

this new sensor, its response to different concentrations of O_2 inside a gas chamber was studied, making the measurement of O_2 in parallel with the Foxy-R probe (Fig. S2.2).

The commercial sensor gives voltage signals (instead of fluorescence intensity). However, the K_{sv} is not sensitive to the units of magnitude used for measuring the O_2 effect on the fluorescence of the fluorophore, so eq. (1) can also be applied but replacing fluorescence intensity (F) by voltage (V). Figure 3 shows the calibration graph obtained with the AuNC@LA-silica platform located in the Luminox™. As can be seen, the results fit the Stern-Volmer equation very well. The K_{sv} obtained was 0.0059 (RSD = 4.9% $n = 3$), quantitatively worse than that of the commercial sensor (0.0369), but approximately in the same proportion as in solution. However, it is less than 2 times lower than that of the Foxy-R, which is due to the physical structure of the sensor. The three K_{sv} used for calculating the averaged value were obtained on three different days with the same AuNC@LA-silica platform, which demonstrates the system stability. As has been indicated, this platform was prepared submitting the silica to three immersion-drying cycles in a AuNC@LA solution. Additional assays were done submitting the support to a higher number of immersion-drying cycles, but no improvements were observed; in fact, for ten cycles the K_{sv} showed a shorter linear response range, probably due to the effect of autoabsorption at high fluorescence intensities. These studies confirm the optimal

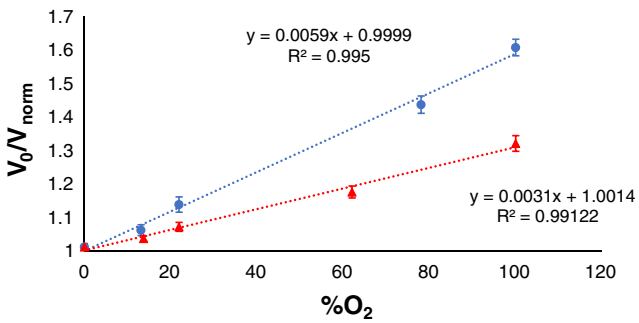

Fig. 3 O_2 effect of the AuNC@LA (blue circle) and AuNC@BSA (red triangle) immobilized on silica support. Signals measured in the Luminox™ sensor ($\lambda_{ext} = 450$ nm and $\lambda_{em} = 680$ nm (LA) or 650 nm (BSA)). The sensor give voltage values. V_0/V_{nor} are the same as F_0/F

fabrication at the established concentration of AuNC@LA (three immersing-dry cycles) as well as the stability and reproducibility of the sensor system for the entire range of % of O_2 in air at room temperature. The reversibility of quenching effects on the AuNC-silica platform has been confirmed, by carrying out several consecutive N_2-O_2 cycles (ESM6.2, Fig. S6.2). Moreover, the O_2 quenching on the AuNC-silica platform was periodically measured during 6 months (after its manufacture) giving reproducible results.

AuNC@BSA immobilized on the silica support were also tested on the Luminox™ O_2 sensor. Figure 3 shows the calibration graph. The K_{sv} obtained was 0.0031% V/V, smaller than that obtained for AuNC@LA. A possible explanation of this result is the fact that the optical arrangement of the Luminox™ sensor (excitation source, filter and detector) are not optimized for the measurement of the fluorescence of the AuNC@BSA, and its LED source (420 nm) is more shifted from its excitation maximum than in the case of AuNC@LA, which causes a loss of sensitivity with this measuring system.

However, the excess protein (BSA) that stabilizes these AuNCs makes it difficult to use them at high temperatures, causing the darkening of the silica platform due to the organic matter burning and making it difficult to measure the fluorescence. Therefore AuNC@LA will be used in the following studies.

Sensing behavior at high temperatures in gas phase

As has been indicated above, one the most interesting possibilities of using AuNCs for O_2 sensing comes from its metallic nature which allows us to use it at temperatures where organic fluorophores decompose. To test this, first the effect of temperature on the AuNC@LA stability and fluorescence was studied, using the system described in the experimental section (ESM2, Fig. S2.1). Once the AuNC@LA-silica was placed inside the optical cell of the pervaporator, the temperature of the resistance was increased from 30 °C to 210 °C (10 °C stepwise) and simultaneously the emission spectra was recorded; after that, the temperature was returned to 30 °C and the cycle was repeated. Figure 4 shows the averaged fluorescence intensity, at the excitation and fluorescence maxima wavelength, at each of these temperatures. As expected, the fluorescence intensity decreased with the temperature, but only during the first cycle. After cooling the cell the intensity slightly increases, and during the second cycle the fluorescence intensity was not dependant on the temperature. This result indicates that during the first cycle, the fluorescence intensity variation was not only due to the expected behaviour but also to some sort of change in the AuNC@LA-silica structure.

This is somehow reflected in the fluorescence spectra (ESM7, Fig. S7.1) which shows slight changes in the 690–700 nm wavelength interval. This result is very important because it demonstrates that, after the first pretreatment, the

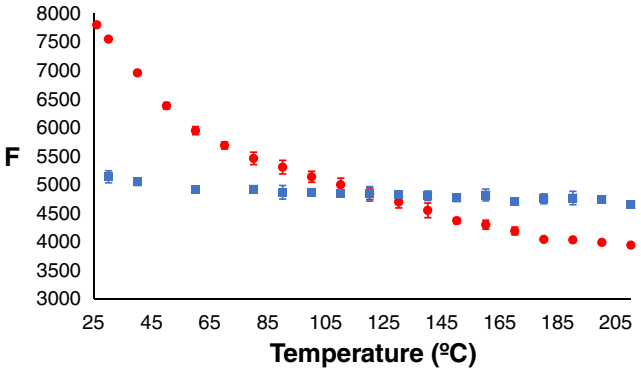

Fig. 4 Average fluorescence of the AuNC@LA-silica emission maximum at each temperature in the pretreatment step. In a 'first cycle' (red circle) of heating from 26 to 210 °C and in a 'second cycle' (blue square), also from 26 to 210 °C ($\lambda_{exc} = 450$ nm, $\lambda_{em} = 690$ nm)

platform can be used as an O_2 sensor at different temperatures without affecting the fluorescence.

In order to study the AuNC@LA-silica response to O_2 at different temperatures, air flows with different oxygen concentrations were passed through the pervaporator where a previously pretreated (after being submitted to the first temperature cycle) AuNC@LA-silica platform was placed; the fluorescence variations were measured with the same optical fiber system as in the previous case. A systematic study was carried out at four temperatures (3 oxygen concentrations at each temperature). By evaluating each of the O_2 concentrations and recording the fluorescence values at the maximum emission of AuNC@LA-silica ($\lambda_{em} = 690$ nm) in each case, we obtained a fluorescence vs $\%O_2$ calibration line for each temperature, from which we derived the different K_{sv} values (Fig. 5). As can be seen, the K_{sv} values were similar from 45 to 100 °C (ESM7.1, Fig. S7.2). It is difficult to predict the temperature effect of the K_{sv}. On the one hand, the higher the temperature, the higher the k_0 (the O_2 diffusion coefficient increases with the temperature). On the other hand, the τ is expected to decrease with the temperature [26, 27] (the non-radiative decay constant increases [28, 29]), so a balanced response is finally observed.

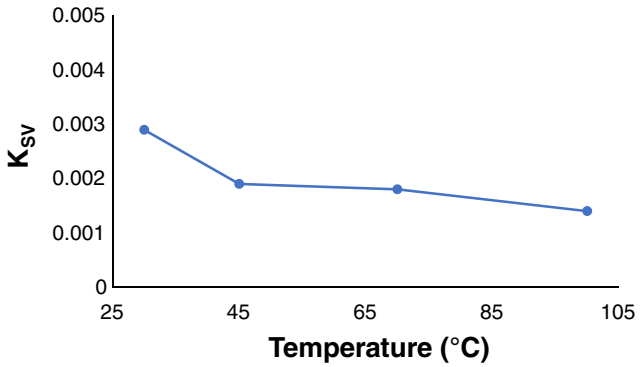

Fig. 5 Temperature effect on the K_{sv} for AuNC@LA-silica ($\lambda_{exc} = 450$ nm, $\lambda_{flu} = 690$ nm)

To demonstrate the ability of the sensor to retain the sensing capability and reversibility after heating, the following experiment was carried out: the K_{sv} was obtained at ambient temperature (from three O_2 concentrations), then the sensor was heated at 100 °C, cooled down at ambient temperature and the K_{sv} was measured again. This cycle was repeated 5 times. The results are detailed in ESM7.2 (Fig. S7.3). As can be seen, no drift is observed and similar K_{sv} values were obtained (RSD = 9.9%,$n = 5$). From the calibration graphs a limit of detection of 3% (V/V) O_2 (3σ) is obtained.

Conclusions

This paper shows that AuNCs can be used as efficient fluorophores in O_2 collisional quenching, following the Stern-Volmer model. AuNC@BSA are more efficient than AuNC@LA but the latter can be used at higher temperatures. Future experiments should be done in order to test the possibility of using AuNCs as an O_2 probe at even higher temperatures. This new type of sensor based on AuNC fluorescence would be an interesting alternative for non-invasive O_2 monitoring in thermically aggressive environments. Considering that the mechanism of the fluorescence quenching is collisional, interferences in the gas phase will come from the same substances as in the case of other O_2 fluorescence based sensors, i.e. paramagnetic species (NO). Working in liquid phase, interferences will come from compounds able to react with AuNCs, especially thiols, so caution should be taken with samples containing these types of components.

Acknowledgements The authors thank to MINECO of Spain (CTQ2016-76846R), DGA-FEDER funding to Research Groups (E74) and BSH (project "Smart Ovens III") for financial support.

Compliance with ethical standards

The authors declare that they have no competing interests.

References

1. Zheng J, Nikovich PR, Dickson RM (2007) Highly fluorescent noble metal quantum dots. Annu Rev Phys Chem 58:409–431
2. Zheng J, Zhou C, Yu M, Liu J (2012) Different sized luminescent gold nanoparticles. Nano 4:4073–4083
3. Wolfbeis OS (2015) An overeview of nanoparticles commonly used in fluorescent bioimaging. Chem Soc Rev 44:4743–4768
4. Cui M, Zho Y, Song Q (2014) Synthesis, optical properties and applications of ultra-small luminescent gold nanoclusters. TrAC Trends Anal Chem 57:73–82
5. Chen LY, Wang CW, Yuan Z, Chang HT (2015) Fluorescent gold nanoclusters: recent advances in sensing and imaging. Anal Chem 87:216–229

6. Li H, Zhu W, Wan A, Liu L (2017) The mechanism and application of the protein-stabilized gold nanocluster sensing system. Analyst 142:567–581
7. Rasheed PA, Lee JS (2017) Recent advances in optical detection of dopamine using nanomaterials. Microchim Acta 184:1239–1266
8. Korotcenkov G, Brinzari V, Cho BK (2016) Conductometric gas sensors based on metal oxides modified with gold nanoparticles: a review. Microchim Acta 183:1033–1054
9. Miller DR, Akbar SA, Morris PA (2014) Nanoscale metal oxide-based heterojunctions for gas sensing: a review. Sens Actuators B Chem 204:250–272
10. Papkovsky DB, Dmitriev RI (2013) Biological detection by optical oxygen sensing. Chem Soc Rev 42:8700–8732
11. Wang X, Wolfbeis OS (2014) Optical methods for sensing and imaging oxygen: materials, spectroscopies and applications. Chem Soc Rev 43:3666–3761
12. Lehner P, Staudinger C, Borisov SM, Regensburger J, Klimant I (2015) Intrinsic artefacts in optical oxygen sensors-how reliable are our measurements. Chem Eur J 21:3978–3986
13. Zou XS, Pan TT, Chen L, Tian YQ, Zhang WW (2017) Luminescence materials for pH and oxygen sensing in microbial cells-structures, optical properties, and biological applications. Crit Rev Biotechnol 37:723–738
14. Wolfbeis O (2015) Luminescent sensing and imaging of oxygen: fierce competition to the Clark electrode. BioEssays 37: 921–928
15. Kenner RD, Khan AU (1976) Molecular oxygen enhanced fluorescence of organic molecules in polymer matrices: a singlet oxygen feedback mechanism. J Chem Phys 64:1877–1882
16. Vishnoi G, Morisawa M, Muto S (1998) A new plastic optical fiber sensor for oxygen based on fluorescence enhancement. Opt Rev 5: 13–15
17. Ghosh RN, Askeland PA, Kramer S, Loloee R (2011) Optical dissolved oxygen sensor utilizing molybdenum chloride cluster phosphorescence. Appl Phys Lett 98:221103
18. Wang Y, Wang Y, Zhou F, Kim P, Xia Y (2012) Protein-protected Au clusters as a new class of nanoscale biosensor for label-free fluorescence detection of proteases. Small 8:3769–3773
19. Das T, Ghosh P, Shanavas MS, Maity A, Mondal S, Purkayastha P (2012) Protein-templated gold nanoclusters: size dependent inversion of fluorescence emission in the presence of molecular oxygen. Nano 4:6018–6024
20. Galbán J, Sanz-Vicente I, Castillo JR, Luque de Castro MD (2001) Integrated analytical pervaporation-gas phase absorptiometry: theoretical aspects and applications. Anal Chim Acta 434:81–93
21. Aldeek F, Muhammed MH, Palui G, Zhan N, Mattoussi H (2013) Growth of highly fluorescent polyethylene glycol-and zwitterion-functionalized gold nanoclusters. ACS Nano 7:2509–2521
22. Lianzhe H, Shuang H, Parveen S (2012) Highly sensitive fluorescent detection of trypsin based on BSA-stabilized gold nanoclusters. Biosens Bioelectron 32(1):297–299
23. Chevrier DM, Chatt A, Zhang P (2012) Properties and applications of protein-stabilized fluorescent gold nanoclusters: short review. J Nanophoton 6:064504
24. Lin CAJ, Yang TY, Lee CH, Huang SH, Sperling RA, Zanella M, Li JK, Shen JL, Wang HH, Yeh HI, Parak WJ, Chang WH (2009) Synthesis, characterization, and bioconjugation of fluorescent gold nanoclusters toward biological labeling applications. ACS Nano 3: 395–401
25. Govindaraju S, Ankireddy SR, Viswanath B, Kim J, Yun K (2017) Fluorescent gold nanoclusters for selective detection of dopamine in cerebrospinal fluid. Sci Rep 7:40298
26. Nakano M, Nagai T (2017) Thermometers for monitoring cellular temperature. J Photochem Photobiol C 30:2–9
27. Shang L, Stockmar F, Azadfar N, Nienhaus GU (2013) Intracellular thermometry by using fluorescent gold nanoclusters. Angew Chem Int Ed Engl 52:11154–11157
28. Jortner J (1971) Radiationless transitions. Pure Appl Chem 27: 389–419
29. Turro NJ (1991) Modern molecular photochemistry. University science books, Mill Valley, California. Ch. 6 p 187